## Title

Measurement and modelling of moisture—electrical resistivity relationship of fine-grained unsaturated soils and electrical anisotropy



## Authors

Merritt, AJ
Chambers, JE
Wilkinson, PB
et al.

## Publication Date

2016

## DOI

10.1016/j.jappgeo.2015.11.005

Peer reviewed

# Measurement and modelling of moisture—electrical resistivity relationship of fine-grained unsaturated soils and electrical anisotropy

Author links open overlay

panel[A.J.Merritt](#)[a][J.E.Chambers](#)[b][P.B.Wilkinson](#)[b][L.J.West](#)[c][W.Murphy](#)[c][D.Gunn](#)[b][S.Uhlemann](#)[bd]
Show more

https://doi.org/10.1016/j.jappgeo.2015.11.005Get rights and content

## Highlights

- Methodology for developing electrical resistivity-moisture content relationships
- Electropetrophysical models of a landslide material.
- Experimental electrical resistivity results show a hierarchy and anisotropy.
- Variation between the fit of experimental data and Waxman–Smits derived petrophysical models.
- Model fit is best for clay-dominated samples but fits less well for sand-dominated samples.

## Abstract

A methodology for developing resistivity-moisture content relationships of materials associated with a clayey landslide is presented. Key elements of the methodology include sample selection and preparation, laboratory measurement of resistivity with changing moisture content, and the derivation of models describing the relationship between resistivity and moisture content.

Laboratory resistivity measurements show that the techniques utilised (samples and square array) have considerable potential as a means of electropetrophysical calibration of engineering soils and weak rock. Experimental electrical resistivity results show a hierarchy of values dependent on sample lithology, with silty clay exhibiting the lowest

resistivities, followed by siltstones and sands, which return the highest resistivities. In addition, finer grained samples show a greater degree of anisotropy between measurement orientations than coarser grained samples.
However, suitability of results in light of issues such as sample cracking and electrical conduction must be identified and accounted for if the results are to be accurately up-scaled to inverted model resistivity results. The existence of directional anisotropy makes model calibration curve selection more difficult due to variability in the range of measured laboratory resistances.
The use of larger measurement array size means that experimental data will be more representative of bulk lithological properties. In addition, use of electrodeswith a relatively high surface area (wide diameter) help maintain low contact resistances and repeat measurement error, relative to narrow electrodes.
Variation exists between the fit of experimental data and petrophysical models. Model fit is best for clay-dominated samples but fits less well for sand-dominated samples. Waxman–Smits equation is appropriately applied in this investigation as all samples have considerable clay mineral content, as is shown in non-negligible CEC results. The incorporation of pressure plate suction measurements on samples, allows suction dissipation to be quantified and evaluated alongside moisture content and electrical resistivity.


- **Previous** article
- **Next** article



## Keywords

Electrical resistivity tomography (ERT)
Electropetrophysics
Landslide study
Soil testing
Unsaturated petrophysical relationships


## 1. Introduction

The moisture content of natural soils is affected by climatic, seasonal and environmental factors such as rainfall amount and intensity, as well as evapotranspiration. Intense rainfall and rapid infiltration is widely accepted as one of the principal landslide triggers as slope materials tend to reduce in shear strength as they reach saturation (Friedel et al., 2006, Cruden and Varnes, 1996, Bell, 2007, Dijkstra and Dixon, 2010, Dijkstra et al., 2014), with a major contributing factor in clay slope instability being the reduction

in pore suction associated with elevated moisture content (Toll et al., 2011, Lourenço et al., 2011).

Electrical Resistivity Tomography (ERT) provides a means of spatially characterising and monitoring the subsurface (Loke et al., 2013, Loke, 1997). It can provide information on lithological variability and is also sensitive to changes in soil moisture content. It is particularly effective when deployed as a time-lapse monitoring tool where, once the influence of temperature has been determined (Hayley et al., 2007), changes in resistivity can be related to subsurface moisture dynamics (Brunet et al., 2010, Chambers et al., 2014, Cassiani et al., 2009). ERT monitoring has therefore proven to be a useful tool for investigating slope hydrology when installed on rainfall-induced landslides (Jongmans and Garambois, 2007, Di Maio and Piegari, 2011, Lebourg et al., 2005, Supper et al., 2014). However, no studies have yet attempted to quantitatively convert electrical resistivity information, recorded from landslide electrical resistivity monitoring, into subsurface soil moisture content.

The relationship between a soil's electrical properties and moisture content vary according to the soils' composition and, in particular, the proportion and type of clay minerals (Shevnin et al., 2007, Russell and Barker, 2010). Consequently, for quantitative moisture content information to be extracted from ERT monitoring results, resistivity-moisture relationships must be modelled using either in-situ or laboratory measurements (Brunet et al., 2010, Binley et al., 2002). In the case of a slope comprising several different lithologies, property relationships linking resistivity and moisture content may need to be determined for each material type.

In this study we consider a methodology for developing resistivity-moisture content relationships of materials associated with a clayey landslide. Key elements of the methodology include sample selection and preparation, laboratory measurement of resistivity with changing moisture content, and the derivation of models describing the relationship between resistivity and moisture content. The samples considered in this study were taken from a shallow slow moving multiple earth slide — earth flow in North Yorkshire, UK. The study site has been the focus of previous geophysical and geotechnical investigations (e.g. Merritt et al., 2013) and ongoing monitoring using 4D ERT. Crucially, it comprises features common to many clayey landslides in Lias mudrocks. It is anticipated that the type of property relationship information derived from this study could eventually be applied to the interpretation of 2D and 3D ERT time series data to quantitatively assess moisture content changes. Quantitative spatial and temporal information on moisture dynamics coupled with geotechnical thresholds

for slope failure (Eichenberger et al., 2013, Sorbino and Nicotera, 2013) could then be used to provide early warning of potential slope instability.

## 2. Methodology

### 2.1. Sample selection and preparation

The landslide considered in this study is located 4 miles west of the market town of Malton, North Yorkshire, UK. The field site is a farm pasture land and is a south-facing hill slope, dipping at approximately 12°. The hill slope is composed of four geological formations of Lower Jurassic and Middle Jurassicage (Fig.1), and – from the top of the slope and decreasing in age – are Dogger Formation (DF), Whitby Mudstone Formation (WMF), Staithes Sandstone Formation (SSF) and located at the base of the slope and occupying the broad embayment is Redcar Mudstone Formation (RMF) (Chambers et al., 2011, Merritt et al., 2013). The landslide system occurs predominantly within the Whitby Mudstone Formation.

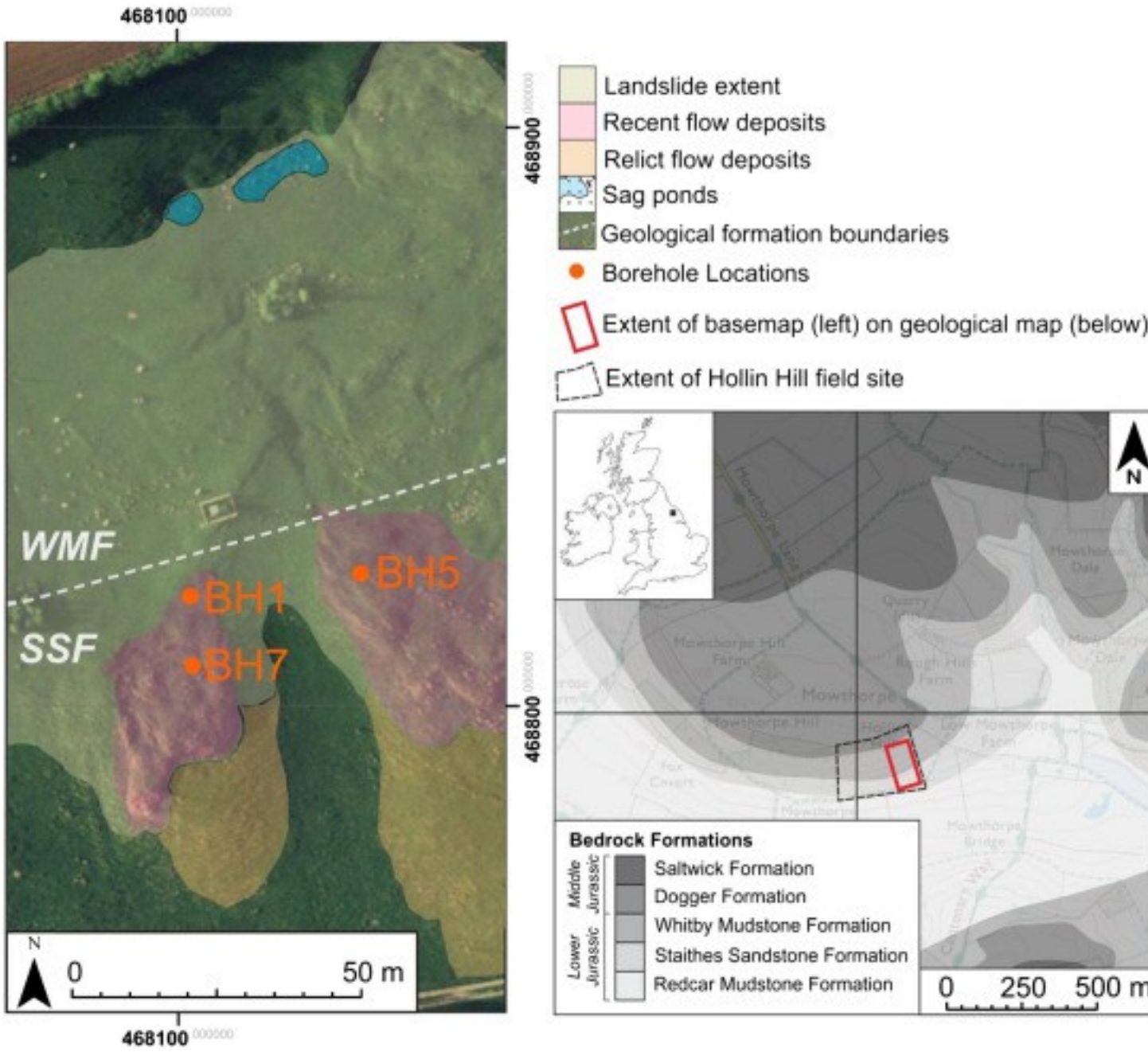


1. Download high-res image (366KB)
2. Download full-size image

Fig. 1. Geological maps of the field site, showing major lithological and geomorphological divisions and borehole locations.

In March 2010 a drilling campaign was undertaken, using a percussion drilling Dando Terrier rig. Eight boreholes were drilled and cores of 0.12 m diameter retrieved. These cores were subjected to geotechnical index testing, including particle size analysis (PSA) (Merritt et al., 2013). Upon completion of the index testing and subsequent

production of core logs (Fig. 2), a series of six samples were extracted from their core, to obtain soil moisture — resistivity relationships through laboratory testing. These 0.14 m long core samples were inserted into sealable, half-core troughs (Fig. 3), thus allowing sample moisture content to be monitored and controlled. The locations of the six samples are displayed in Fig. 2 and were selected to be representative to the major lithologiesassociated with the landslide. In addition, gradational boundaries were avoided as were localised structural features such as landslide shear surfaces.

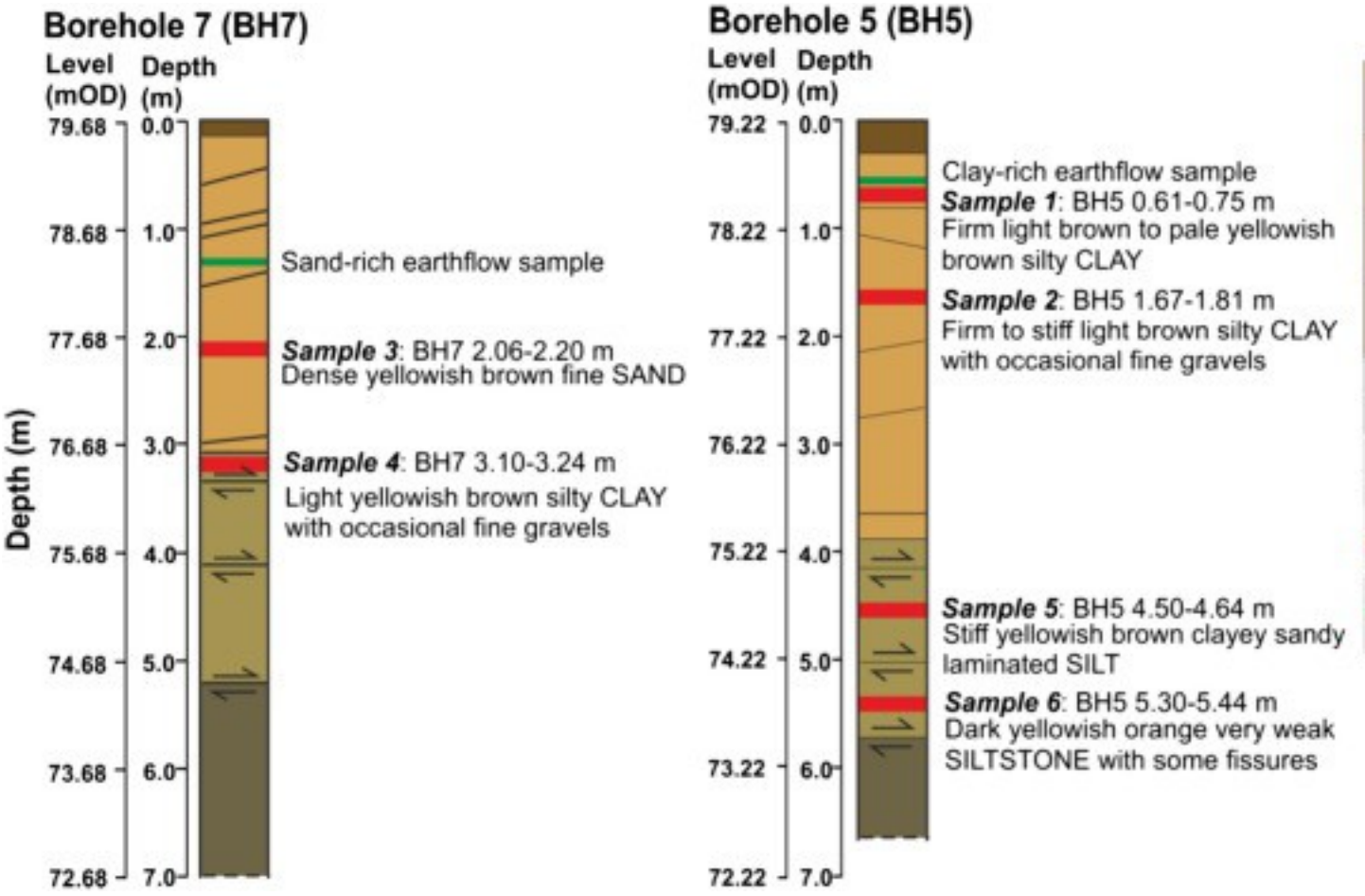


1. Download high-res image (234KB)
2. Download full-size image

Fig. 2. Location and depth of soil samples selected for laboratory electrical resistivity measurements and suction testing (by pressure plate). Presented core logs are interpreted in terms landslide deposit type and are adapted from Merritt et al. (2013).

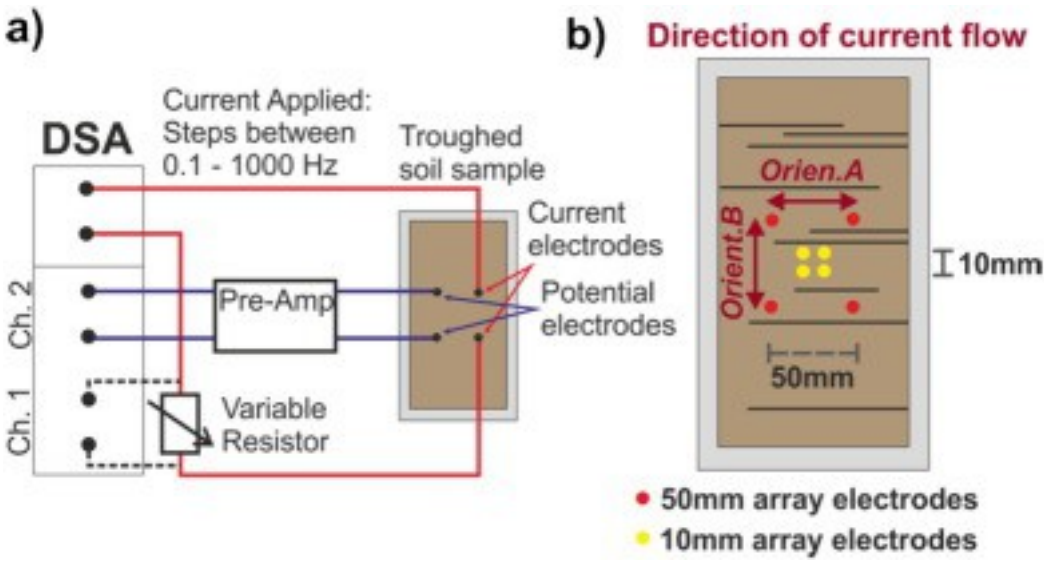


1. Download high-res image (92KB)
2. Download full-size image

Fig. 3. a) (left) Electrical circuit diagram of Digital Signal Analyser circuit board and pre-amplifier experimental setup (adapted from Ntarlagiannis et al., 2005). b) (right) Diagram of sample trough along with electrode array locations, measurement dimensions and current flow directions.

2.2. Measurement procedure

The electrical resistance of soil samples (and saline solutions used during trough calibration) were measured using National Instruments NI-4461 digital signal analyser (DSA) linked to a preamplifier and variable resistor (Fig. 3). The instrument is similar to that employed by Slater and Lesmes (2002) and provides a means of undertaking a four-point measurement of transfer resistance. Measurement of the potential was made in the frequency-domain in the range of 0.1 Hz to 1000 Hz. A reference resistance was matched to the initial cell resistance (at 1000 Hz) and a comparison was made between the measured waveform at the potential electrodes with that across the reference resistor (Vanhala and Soininen, 1995). The waveform difference was recorded as decibel noise, dB, and the relationship between decibel noise and the initial cell resistance is a power law

$$\Omega fn=\Omega Ref\times 10Nfn/20$$

Equation 1. Sample electrical resistance at frequency, $\Omega_{(fn)}$, as a function of cell resistance, $\Omega_{Ref}$ and magnitude of recorded noise as a function of frequency, $N_{(fn)}$.

The resistance measurement was made using the square array measurement type (see Fig. 3a). For practical reasons, the electrode array was placed directly into the

open, upper surface of the half-core. As with the methodology introduced in Russell and Barker (2010), two measurement array sizes were made, a 50 mm (5 cm) and a 10 mm (1 cm) square array. These two electrode array sizes were implemented to investigate the effects of sedimentary structure and fissuring of varying scales. A total of four measurements were made for each array size and each moisture content, by positioning the measurement array electrode guide in the same position in the sample each time.
Constant electrode penetration depth was maintained throughout the resistance measurement, and electrodes were given a slight taper to minimise sample disturbance during insertion. Electrodes were composed of two materials; 50 mm array electrodes were composed of 4 mm diameter stainless steel (grade 316) and penetrated 25 mm and the 1 cm array electrodes were composed of 2 mm diameter silver alloy (Ag) and penetrated 40 mm.

In addition to two array sizes (Fig. 3b), electrical measurements were performed in two orientations, one parallel (Orientation A) and one perpendicular to bedding (Orientation B), thus allowing analysis of directional anisotropy of electrical resistivity attributed to the effect of sedimentary structure. The main difference between the method utilised here and that used by Russell and Barker (2010) is that here, repeated measurements in each orientation are performed to estimate measurement errors, and that measurements were taken on undisturbed soil core samples, instead of reconstituted soil. The benefit of testing undisturbed samples is that variation in electrical properties attributed to sedimentary structure can be investigated.
Electrical resistance measurements performed on the soil samples were converted to electrical resistivity through applying a geometric factor, *k*. This conversion factor was determined by filling troughs with a series of NaCl saline solutions of known electrical conductivities (measured using conductivity probe) and measuring the solution resistance using the laboratory DSA and pre-amplifier. Linear interpolation of the solutions' electrical resistivities and respective resistances was used to determine *k*.
$$k=\rho a/R$$
Equation 2. Relationship between apparent resistivity ($\boldsymbol{\rho}_a$), resistance ($\boldsymbol{R}$) and geometric factor ($\boldsymbol{k}$).
Care was taken to ensure that the saline solution resistivities were representative of the range of sample resistivities to confirm that the geometric factor is independent of the sample resistivity. Fig. 4 shows the relationship between solution electrical resistivity

and measured resistance, along with geometric factor, for each of the electrical measurement orientations performed.

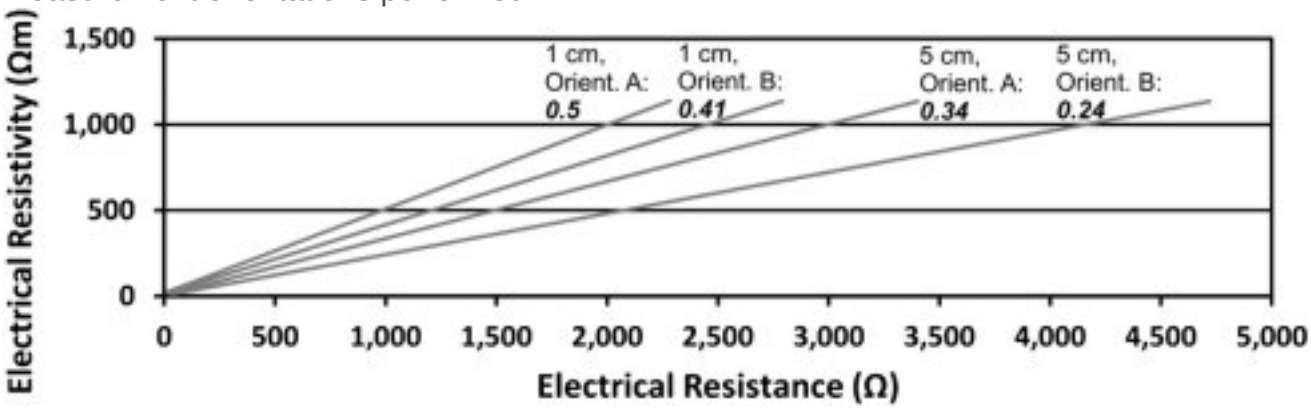


1. Download high-res image (81KB)
2. Download full-size image

Fig. 4. Relationship between saline solution electrical resistivity ($\rho_a$), measured electrical resistance ($R$) and calculated geometric factor ($k$) for each electrode array size and measurement orientation.

Sample temperatures were monitored throughout the experiments using a thermometer probe. All electrical measurements were normalised to the mean air temperature (MAT, °C) at the Hollin Hill field site, 10 °C. The conversion between the measured sample temperature in the laboratory and MAT was made assuming that 2% $\Delta \rho = 1\ °C^{-1}$ (Hayley et al., 2010, Hayley et al., 2007, Chambers et al., 2014, Brunet et al., 2010).

Samples were incrementally air-dried in steps of between 2% and 5% from ambient moisture content, and a further set of resistance measurements performed on all samples at their new moisture content. The gravimetric moisture content of the soil was determined at each drying increment and was determined by

G=mw-md/md

Equation 3. Formula for determining soil gravimetric moisture content, $G$, where, $m_w$ is the incremental weight of soil and $m_d$ is the dry weight of the soil (Head, 2002).

After the samples reached their lowest dry weight by air-drying they were progressively re-wetted with de-ionised water and resistances were measured. Care was taken to perform several resistance measurements at moisture contents within the range already tested during incremental drying, thus highlighting clear reciprocity (and any hysteresis present) between resistance measurements. Upon re-wetting beyond ambient moisture content, until water pooled on the sample surfaces, soil samples were oven dried at 50 °C until completely dry (no more loss of mass) and the sample dry

weight was determined by a precise mass balance. Samples were not oven dried at 105 °C as per Head (2002) as the PVC troughs would have melted.
Repeat measurements were performed at half of the moisture content increments for each of the six samples. Resistivity measurement error assessment is more understandable if the repeat measurement error is represented as a percentage of the forward resistivity ($\rho_f$) measurement, with percentage errors, calculated as, and where repeats resistivity ($\rho_r$):

$$ER\% = \rho f - \rho r / 2 / \rho f) \cdot 100$$

Equation 4. Repeat measurement percentage error $E_{R\%}$ analysis of sample resistivity measurements.

### 2.3. Electropetrophysical modelling

Several approaches have been developed for modelling the relationship between resistivity — moisture content of geological materials. Two of the most commonly applied are Archie's Law (Archie, 1942, Glover et al., 2000), which accounts electrical conductance through the electrolyte, and the Waxman–Smits model (Waxman and Smits, 1968), which also accounts for electrical conduction in the electrical double layer (EDL), near clay mineral surfaces. Due to the clayey nature of the samples considered here, the Waxman–Smits model has been applied in this study.
The original Waxman and Smits equation (Waxman and Smits, 1968) is given as

$$\rho = FSn1\rho w + BQvS - 1$$

Equation 5. Original Waxman–Smits Equation.

where $\rho$ is formation resistivity, $S$ the formation saturation, $n$ a saturation exponent, $F$ the formation factor, $\rho_w$ is the pore fluid resistivity, $B$ the average mobility of the ions and $Q_v$ is the cation concentration per unit pore volume (meq $cm^{-3}$) of the EDL (Revil et al., 1998a). The surface conductivity (S $m^{-1}$) can be expressed as the product of $Q_v$ and $B$

$$\sigma s = BQv$$

Equation 6. Surface conductivity in the Electrical Double Layer of clay minerals.

Cation exchange capacity, $c$,has units meq/100 g, and average mobility of the ions, $B$, is commonly described as the equivalent conductivity of the compensating counterion, (S $m^{-1}$) $cm^3$ $meq^{-1}$. $Q_v$ and (Revil and Glover, 1998b, Brovelli et al., 2005) are determined by

$$Qv = 1 - \varphi \rho gc / 100\varphi$$

Equation 7. Cation concentration per unit pore volume, $Q_v$

B=4.61-0.6Exp-σw/1.3

Equation 8. Average mobility of cations, $B$, SI units of (S $m^{-1}$) $cm^3$ $meq^{-1}$ and where units of $\sigma_w$ are S $m^{-1}$.

The Waxman–Smits equation can be modified to incorporate gravimetric moisture content ($G$, GMC) rather than saturation (Chambers et al., 2014), i.e.,

ρ=Fφρw1-φρgGnσw+Bcρw100G-1

Equation 8. Modified Waxman–Smits equation, where $c$ is cation exchange capacity in meq/100 g.

where, $\varphi$ is the soil porosity, $\rho_w$ is the water density (assumed to be 1 g $cm^{-3}$), $\rho_g$ is the particle density, g $cm^{-3}$, and $G$ is soil gravimetric moisture content (GMC), %. In this study, the electrical conductivity of the pore fluid (groundwater), $\sigma_w$, S $m^{-1}$, was established using the Solinst LTC Levelogger Junior, a down hole installed piezometer which was installed in the flow region of the Hollin Hill landslide system. An average pore fluid conductivity of 0.098 S $m^{-1}$ (10.13 Ωm) was determined over a 10-month logging period. Pore fluid conductivity it observed to vary between 9.06 Ωm and 11.10 Ωm during the logging period, such variation magnitude leads to a negligible effect on Waxman–Smits Modelling.

The original form of Waxman–Smits equation relates moisture content to saturation using soil porosity. Clay rich soils, such as the Whitby Mudstone Formation investigated at Hollin Hill, exhibit variable porosity with change in moisture content, attributed to the shrink-swell capability of certain clay minerals. Porosity was assumed constant during modelling, and appears as a multiplicative factor in the modified Waxman–Smits Equation that only affects the formation factor. The formation factor is itself one of the fitting parameters of the resistivity-moisture content curve.

Geotechnical parameters, $c$, $\varphi$ and $\rho_g$ were determined through geotechnical testing. These input parameters were passed to the Waxman–Smits model to determine $F$ and $n$. The curve was iteratively fitted using the ‘findMinimum’ function of Mathematica.

## 2.4. Waxman–Smits modelling

Where no data was available to constrain the saturation factor ($n$) an arbitrary value of 2 (Telford et al., 1991) is often assigned to this parameter. However, this value does vary between models and examples of saturation exponent from literature vary between 1.0 and 2.87 (Ulrich and Slater, 2004). Saturation ($n$) and formation factors ($F$) are fitted

parameters of modified Waxman–Smits equation, the equation applied in this investigation.

The Waxman–Smits modelling procedure was performed a total of 36 times for all samples, and wetting and drying curves were fitted together due to the lack of hysteresis between measurement data. Each of the six samples had two sets of resistivity measurements modelled, one applied to the 50 mm array, the other to the 10 mm array. Each of the two array sizes had two orientations curve-modelled (orientations A and B) as well as their arithmetic average. Cation exchange capacity values range between 25.90 meq/100 g, for the silty clay of Sample 1 and 6.40 meq/100 g for the sand of Sample 3. Porosity is seen to vary between 0.47 for the silty clay of Sample 1 and 0.32 for the siltstone of Sample 6 and particle density varies slightly between 2.69 and 2.74, Table 1. Petrophysical model errors are presented in Table 2.

Table 1. Results of Waxman–Smits modelling of electropetrophysical properties of landslide material. Where, $B$ and $\sigma_w$ are input parameters and 2.04 (S $m^{-1}$) $cm^3$ $meq^{-1}$and 0.098 S $m^{-1}$ respectively. $\rho_w$ is water density and is assumed to be 1 g $cm^{-3}$.

| | | | 50 mm array | | | 10 mm array | | |
|---|---|---|---|---|---|---|---|---|
| **Model input parameters** | | **Waxman–Smits model fitted parameters** | | | | | | |
| Sample 1 | | | | | | | | |
| **CEC, c** | 25.9 | | Average | Orient. A | Orient. B | Average | Orient. A | Orient. B |
| **Porosity, ϕ** | 0.5 | F | 21.0 | 12.0 | 30.0 | 21.0 | 14.2 | 24.7 |
| **Density $\rho_g$** | 2.7 | n | 2.1 | 1.7 | 2.2 | 2.1 | 1.9 | 2.3 |
| Sample 2 | | | | | | | | |
| **CEC, c** | 19.2 | | Average | Orient. A | Orient. B | Average | Orient. A | Orient. B |
| **Porosity, ϕ** | 0.4 | F | 21.5 | 17.4 | 25.1 | 19.6 | 16.1 | 22.2 |
| **Density $\rho_g$** | 2.7 | n | 2.1 | 2.0 | 2.2 | 2.4 | 2.1 | 2.6 |
| Sample 3 | | | | | | | | |
| **CEC, c** | 6.4 | | Average | Orient. A | Orient. B | Average | Orient. A | Orient. B |
| **Porosity, ϕ** | 0.4 | F | 59.8 | 73.1 | 58.2 | 54.3 | 53.9 | 53.3 |
| **Density $\rho_g$** | 2.7 | n | 2.4 | 2.0 | 2.6 | 2.6 | 2.6 | 2.6 |
| Sample 4 | | | | | | | | |
| **CEC, c** | 6.6 | | Average | Orient. A | Orient. B | Average | Orient. A | Orient. B |
| **Porosity, ϕ** | 0.3 | F | 22.2 | 20.4 | 23.9 | 16.4 | 20.3 | 10.8 |
| **Density $\rho_g$** | 2.7 | n | 1.9 | 1.9 | 1.9 | 1.9 | 1.9 | 1.8 |

| | | | 50 mm array | | | 10 mm array | | |
|---|---|---|---|---|---|---|---|---|
| **Model input parameters** | | | **Waxman–Smits model fitted parameters** | | | | | |
| Sample 5 | | | | | | | | |
| **CEC, c** | 10.0 | | Average | Orient. A | Orient. B | Average | Orient. A | Orient. B |
| **Porosity, ϕ** | 0.3 | F | 47.3 | 32.1 | 62.3 | 60.1 | 29.6 | 86.3 |
| **Density $\rho_g$** | 2.7 | n | 1.9 | 1.8 | 1.9 | 2.0 | 1.6 | 2.2 |
| Sample 6 | | | | | | | | |
| **CEC, c** | 12.0 | | Average | Orient. A | Orient. B | Average | Orient. A | Orient. B |
| **Porosity, ϕ** | 0.3 | F | 83.6 | 31.0 | 129.0 | 60.1 | 58.3 | 63.0 |
| **Density $\rho_g$** | 2.7 | n | 3.1 | 2.4 | 3.3 | 2.0 | 2.3 | 3.0 |
| Sample 6 (crack affected measurements excluded) | | | | | | | | |
| **CEC, c** | 12.0 | | Average | Orient. A | Orient. B | Average | Orient. A | Orient. B |
| **Porosity, ϕ** | 0.3 | F | 72.1 | | 105.6 | | | |
| **Density $\rho_g$** | 2.7 | n | 3.2 | | 3.3 | | | |

Table. 2. Waxman–Smits model misfit errors between laboratory experimental data and petrophysical model. Misfit errors are recorded as percentage root-mean-square error(%RMS).

| | 50 mm square array | | | 10 mm square array | | |
|---|---|---|---|---|---|---|
| | **Average** | **Orient. A** | **Orient. B** | **Average** | **Orient. A** | **Orient. B** |
| **Sample 1, %RMS** | 42.6 | 31.3 | 50.6 | 26.8 | 57.1 | 23.7 |
| **Sample 2, %RMS** | 21.5 | 34.7 | 18.5 | 30.9 | 56.7 | 35.7 |
| **Sample 3, %RMS** | 92.2 | 68.2 | 108.2 | 113.6 | 104.6 | 132.8 |
| **Sample 4, %RMS** | 27.0 | 33.7 | 22.8 | 83.5 | 58.7 | 205.4 |
| **Sample 5, %RMS** | 27.0 | 35.0 | 25.4 | 32.2 | 58.9 | 30.0 |
| **Sample 6, %RMS** | 35.8 | 76.0 | 41.8 | 52.4 | 49.0 | 84.1 |
| **Sample 6 (excluding crack affected), %RMS** | 31.5 | 76.0 | 33.9 | 52.4 | 49.0 | 84.1 |

## 2.5. Soil moisture, matric suction & electrical resistivity

It is widely assumed that most landslides are triggered by rainfall (Cruden and Varnes, 1996), and that landslide events can often be correlated with rainfall events; however, it is the changes in pore water pressures as a consequence of rainfall infiltration which are the cause of slope activations (Toll et al., 2011). When rainfall infiltrates, the suctional forces, or negative pore water pressures, which under normal conditions act to increase the strength and therefore stabilise the soil, and reduce the frictional

component of the soils strength(Barnes, 2010). It is these seasonally and temporally transient near surface pore water pressure changes that, if sufficiently large can induce landslides (Toll et al., 2011).

We have therefore also considered the relationship between pore suction and moisture content for samples recovered from the study site. To achieve this we developed soil water retention curves via the pressure outflow method using a Pressure Plate apparatus. Two samples of about 0.5 kg were extracted from the core within active flow material of BH5 and BH7 (their exact locations relative to landslide structure are shown in Fig. 3). The two samples originated from BH5 0.4 m and BH7 1.3 m. Both were saturated by immersion in water for a week until visibly saturated. Six cylindrical plastic trays (10 mm deep and 40 mm wide) were weighed and placed on to the surface of the porous pressure plate apparatus. A small square of kitchen roll was placed into the tray to act as a base for the saturated soil samples and sit between the porous plate and the sample yet still permit hydraulic connectivity between soil and plate. Three of the six trays were filled with the clay earthflow material of BH5 0.4 m, the other three filled with sandier earthflow material of BH7 1.3 m. Each filled tray was weighed and re-placed onto the plate before closing and sealing the pressure plate apparatus and commencing suction testing over a pressure range of 1100 kPa.

Here, pore water pressure variations (due to matrix suction development and dissipation) related to changes in moisture content as soil samples are wetted/dried are quantified in the laboratory. These GMC-suction measurements are then converted to electrical resistivity, using an appropriate Waxman–Smits model and an assessment is made of the suitability of ERT as a proxy for soil suctions.

## 3. Results

### 3.1. Laboratory measurements

All of the six samples exhibit a general trend of increasing resistivity with decreasing gravimetric moisture content (Fig. 5, Fig. 6). This increase in resistivity is most pronounced for the fine sand of Sample 3 (Fig. 5), which shows a resistivity increase of four orders of magnitude with only a 4% moisture content change (between 1% and 5% GMC). The clays of Samples 1 and 2 (Fig. 5) also show increases in soil resistivity with decreasing moisture content, however, the magnitude of resistivity increases – at the lowest MC – are much less abrupt than Sample 3, with a 100–150 Ωm increase taking place over a moisture content decrease of 20% (at lowest GMC). The silt and siltstone of Samples 5 and 6 (Fig. 6) exhibit a resistivity increase of 2–3 orders of

magnitude over a moisture content range of 10% (at lowest GMC) and shows intermediate responses, between the large increases in resistivity at low moisture contents of the Sample 3 (sand), and the much smaller resistivity increases at low moisture contents seen for the clays of Samples 1 and 2.

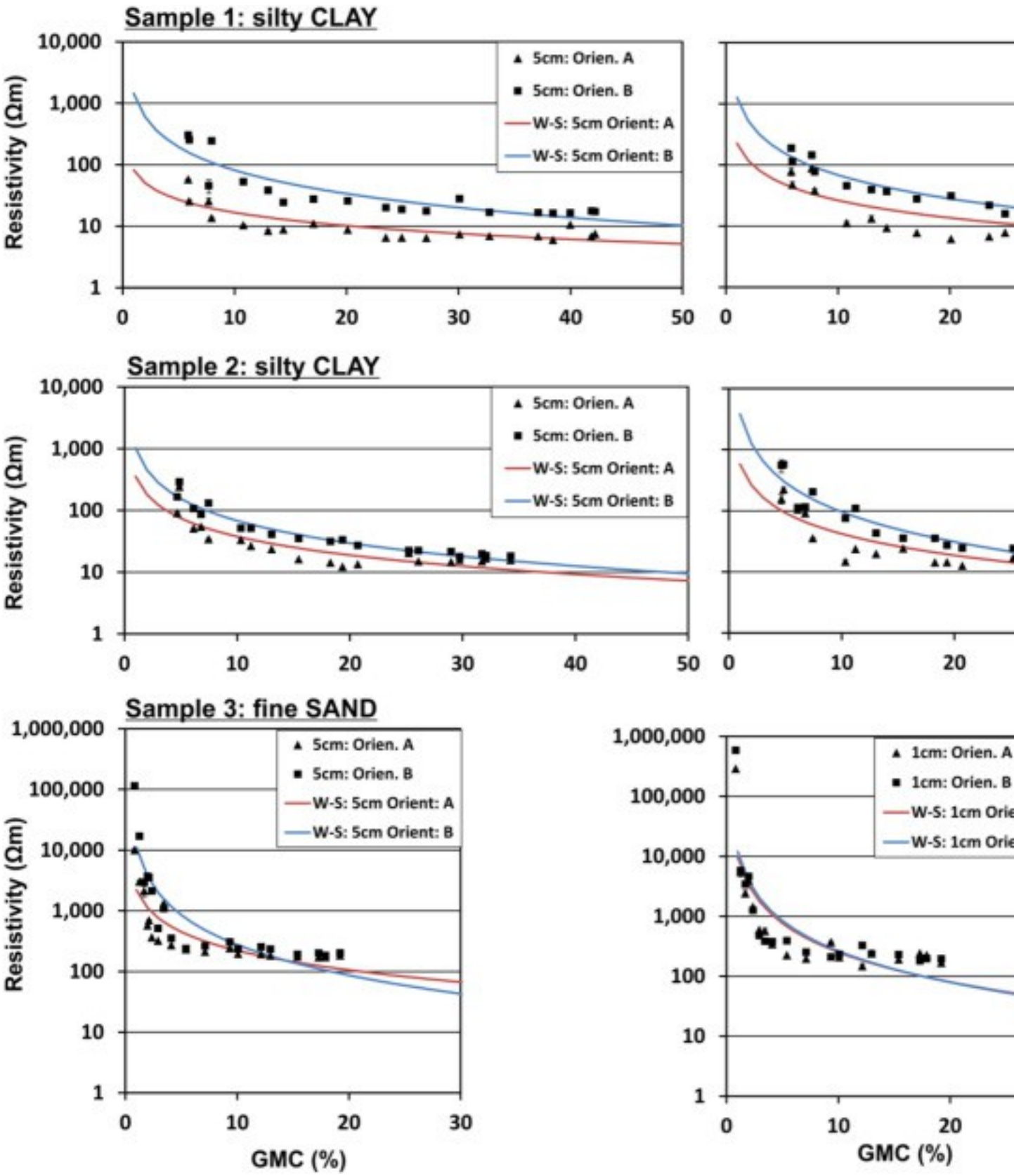


1. Download high-res image (295KB)

2. Download full-size image

Fig. 5. Electrical resistivity — soil moisture content relationship of earthflow deposits of the Hollin Hill landslide system. Presented are the associated Waxman–Smits models for each of the electrical measurement orientations.

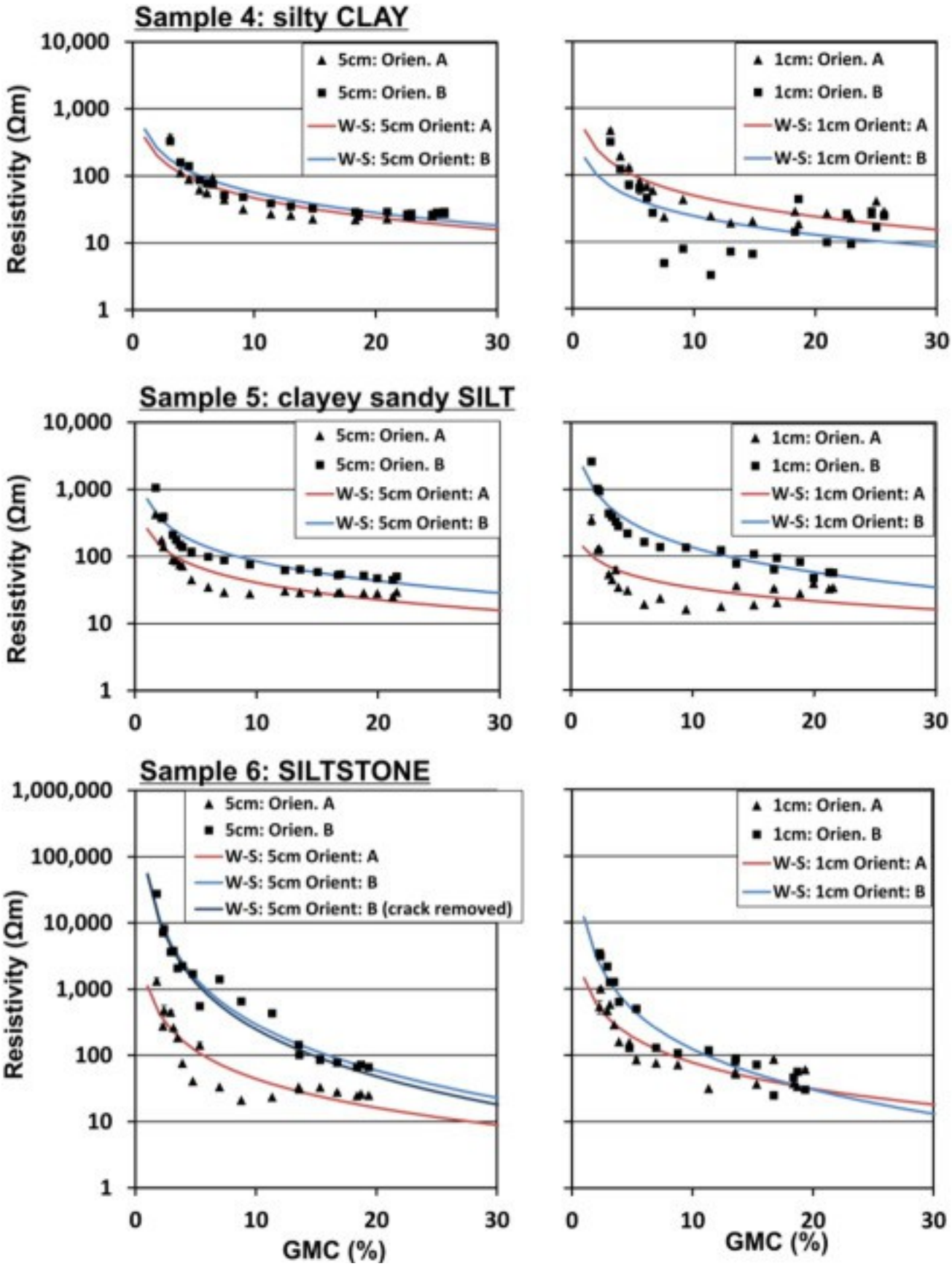
Sample 4: silty CLAY
Resistivity (Ωm)
10,000
1,000
100
10
1
0
10
20
30
5cm: Orien. A
5cm: Orien. B
W-S: 5cm Orient: A
W-S: 5cm Orient: B
1cm: Orien. A
1cm: Orien. B
W-S: 1cm Orient: A
W-S: 1cm Orient: B
Sample 5: clayey sandy SILT
Resistivity (Ωm)
10,000
1,000
100
10
1
0
10
20
30
5cm: Orien. A
5cm: Orien. B
W-S: 5cm Orient: A
W-S: 5cm Orient: B
1cm: Orien. A
1cm: Orien. B
W-S: 1cm Orient: A
W-S: 1cm Orient: B
Sample 6: SILTSTONE
Resistivity (Ωm)
1,000,000
100,000
10,000
1,000
100
10
1
0
10
20
30
GMC (%)
5cm: Orien. A
5cm: Orien. B
W-S: 5cm Orient: A
W-S: 5cm Orient: B
W-S: 5cm Orient: B (crack removed)
1cm: Orien. A
1cm: Orien. B
W-S: 1cm Orient: A
W-S: 1cm Orient: B
GMC (%)

1. Download high-res image (274KB)
2. Download full-size image

Fig. 6. Electrical resistivity — soil moisture content relationship of slump deposits and in-situ material of the Hollin Hill landslide system. Presented are the associated Waxman–Smits models for each of the electrical measurement orientations.

The two electrode array sizes that were considered during soil resistivity measurement and results reveal several trends. Firstly, resistivity at specific moisture content varies with both array size and measurement orientation. It can be seen that the measurements perpendicular to bedding, for both the 50 mm and 10 mm arrays, generally return higher resistivity values than the measurements parallel to bedding. The exception to this trend is the silty clayof Sample 4 whose results from the 10 mm array and oriented parallel to bedding return the lowest resistivity values for much of the moisture content range. Sample 3 (sand) shows divergence of resistivity values between the 50 mm and 10 mm array sizes at the drier end of the moisture content scale, and minimal resistivity difference between measurement orientations. Resistivities for both array sizes and measurement orientations of Samples 1 and 2 exhibit little scatter throughout the moisture content range.

The relationship between resistivity, electrode orientation and moisture content is less clear for Sample 4. The silty clay soil of Sample 4 (Fig. 6) exhibits little scatter in resistivity both between measurement orientations and electrode array sizes over the majority of the moisture content range. However, between 4% and 12% moisture content the 10 mm, bedding-perpendicular orientated resistivity measurement is lower than might be expected with respect to their surrounding resistivity values. Soil resistivity values from Sample 4 show very little divergence (with the exception of the 10 mm, bedding-perpendicular orientated resistivities described previously) between values from the two square array sizes.

The clayey, sandy laminated silt of Sample 5 shows bedding-perpendicular orientated resistivity values consistently higher than those orientated bedding-parallel. Resistivity values for a specific measurement orientation do not show the same degree of coincidence as the other samples, there is a clear difference between the resistivities measured between the 50 mm and 10 mm array sizes and this difference is exhibited by all measurements carried out on Sample 5. Resistivity measurements utilising the 10 mm array produce the highest and lowest values, with the two 50 mm array measurements positioned between the minimum and maximum 10 mm derived values.

Conversely, it is the 50 mm array which produces the highest and lowest resistivity values of Sample 6. This apparent disparity between two lithologically similar samples can be explained in terms of the pervasiveness, scale and range of soil drying processes such as soil desiccation. In terms of electrical resistivity, the silts and siltstones of Samples 5 and 6 plot between the higher resistivities of Sample 3 and the lower resistivities of Samples 1, 2 and 4.

Electrical resistivity results show a hierarchy of values dependent on sample lithology, with silty clay exhibiting the lowest resistivities, followed by siltstones and sands, which return the highest resistivities. In addition, finer grained samples show a greater degree of anisotropy between measurement orientations than coarser grained samples. Repeat percentage errors for resistivity measurements reveal that repeat errors are highest for resistivity measurements performed at the lowest gravimetric moisture contents (GMC). Measurements using the 10 mm square array almost consistently provide the highest repeat error throughout, as errors using the equivalent 50 mm square array are often up to five times lower. Repeat measurement errors of the 50 mm array are consistently lower than those from the 10 mm square array, which appear to vary much more sporadically with only small changes in moisture content. The repeat electrical measurementerror ranges between 5% for all samples at the highest GMC but generally rise to 15% at the lowest GMC (~ 1–5% GMC). Several repeat measurement outliers exist at low GMC of up to 25%.

### 3.2. Electropetrophysical modelling

Mirroring laboratory electrical results, Waxman–Smits models fitted to these data are in accordance with many of the trends observed in laboratory results. Models pertaining to bedding-perpendicular measurements consistently return higher resistances than bedding-parallel, with the only exception being Sample 4, 10 mm array. Several models converge at the higher end of the GMC range, Sample 3, 50 mm and Sample 6, 10 mm exhibit this model feature. Models are presented as red and blue solid lines on Fig. 5, Fig. 6, along with resistivity measurement results. Model fitting parameters and input parameters are displayed in Table 1.
In order to quantify the effect of cracking on the electro-petrophysical model of Sample 6 and bedding-perpendicular, the modelling was performed a second time (Fig. 6, Table 1). The removal of crack affected laboratory measurements reduces the model's resistivities slightly at high GMC but remains consistent with the crack affected model at low GMC.

Model error is a measure of the misfit between experimental data and associated petrophysical model and in this investigation ranges between 18.5% and 205%. The bedding-parallel, 10 mm square array measurements records %RMS errors almost consistently double those associated with the 50 mm array, an example being Sample 1, 57.1% and 31.3% respectively. Sample 6 is the only exception to this trend, as 50 mm (orient. A, bedding-parallel) %RMS is higher than 10 mm at 76.0% and 49.0%.

Errors associated with bedding-perpendicular measurements generally follow this pattern, as Sample 1 orientation B is the only sample which records a %RMS error higher for 50 mm array than 10 mm array. Removing crack affected experimental data from the 50 mm array model decreases the %RMS from 41.8% to 33.9%.

The fine sand of Sample 3 records some of the highest %RMS errors of the investigation, ranging between 68.2% and 132.8%. The 10 mm array model errors pertaining to Sample 4 are high relative to their 50 mm array model errors, falling between 58.7% and 205.4% and are considered further in the discussion.

Model curve errors are therefore generally higher for the 10 mm array and for the sand samples, compared to silty clay samples, and are attributed to contact resistance issues.

### 3.3. Soil moisture retention & electrical resistivity relationships

Soil moisture retention curves are presented in Fig. 7. The two samples, when compared, show several similarities and differences. Firstly, the clay-rich earthflow material of BH5 has a much higher gravimetric moisture content range than the sand-rich earthflow material of BH7, ranging between 30.5%–49.2% and 10.6%–18.7% respectively for the pressure range tested. Thus, indicating the differing abilities to retain soil moisture in quasi-static conditions. Both samples reveal that moisture contents reduce relatively rapidly at low suctions (100–400 kPa), but as suctions increase beyond 400–600 kPa moisture contents incrementally reduce by much less. Using the sand of BH7 as an example; a suction increase from 100 kPa to 300 kPa results in a moisture content decrease of 2.4% change in GMC, as oppose to between 900 kPa to 1100 kPa which saw GMC drop by just 1.2%.

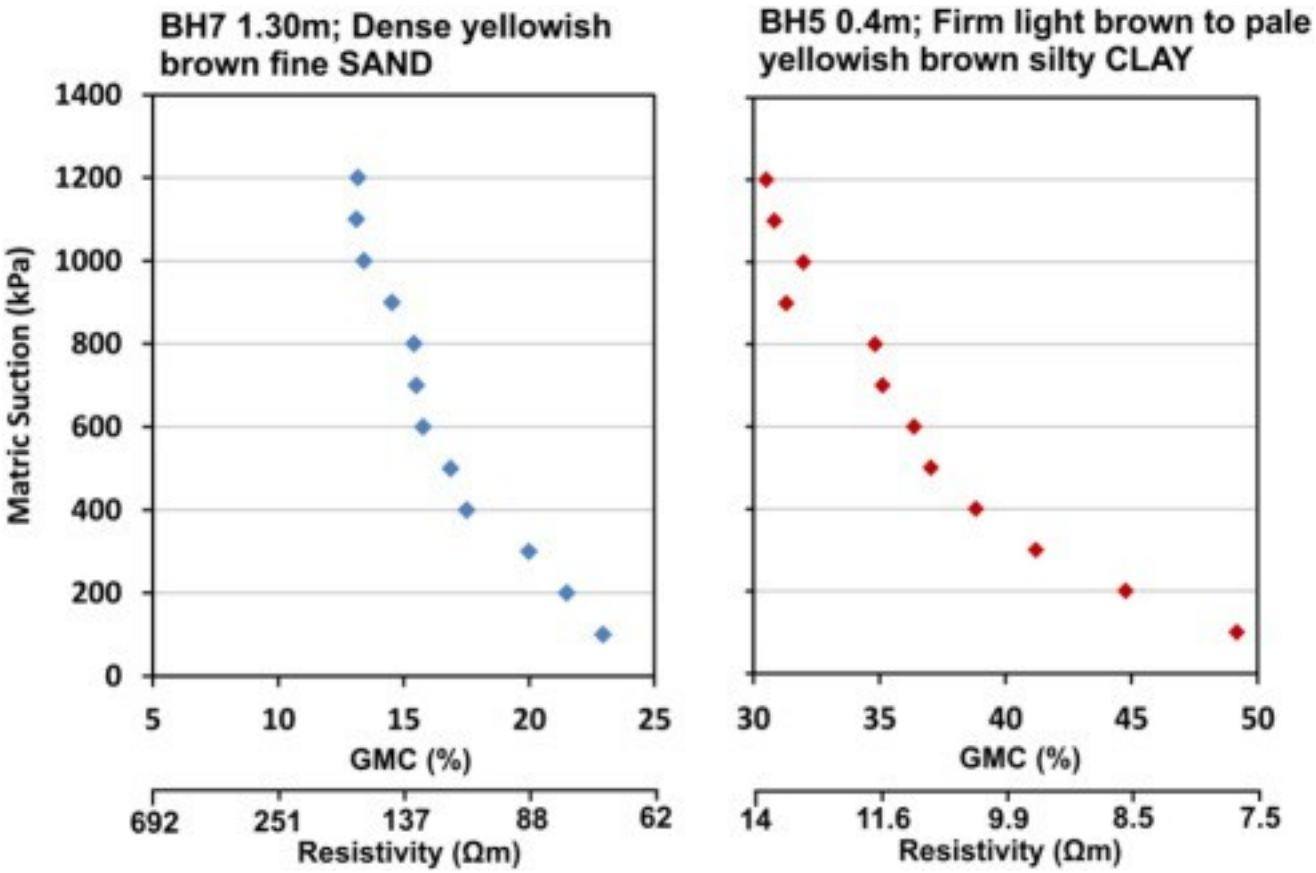


1. Download high-res image (105KB)
2. Download full-size image

Fig. 7. Soil moisture retention curve of two earthflow samples, extracted from Hollin Hill soil cores. a) (left) BH7,1.30 m, and b) (right) BH5, 0.40 m. NB, non-linear electrical resistivity axes.

The range of resistivities exhibited throughout the suction measurements is markedly different between the two samples. The clay has relatively low resistivities of between 7.7 Ωm at high GMC to 13.6 Ωm at low GMC. In contrast, the sand of BH7 records much higher resistivities for the same suction range between 98.4 Ωm at high GMC to 228.4 Ωm at low GMC.

The results of soil moisture retention measurements reveal that the suctions pertaining to the sand rich flow material (Fig. 7) varies over narrow range of moisture contents, but that these correspond to a wider range of resistivity compared to the clay flow.

## 4. Discussion

### 4.1. Electrical properties of landslide materials

The six samples all show that soil resistivity increases as soil moisture content decreases. This relationship can be attributed to the manner in which electrical current flows through the soil samples as a function of soil moisture content. The geological materials tested here are soils and weak sedimentary rocks. They are granular and exist as a solid mineral assemblage phase with associated pore fluid, i.e. air and water. The flow of electrical current is predominantly within the pore fluid as movement of charged ions in the electrolyte. In clay rich soils there will also be a significant component of flow within the EDL associated with clay mineral surfaces.

Almost without exception, bedding-perpendicular measurements record higher resistivities than their bedding-parallel equivalents. This feature is attributed to the orientation of current flow relative to the prevailing sedimentary structure of the sample, structure such as bedding and preferential alignment of platy minerals.

This anisotropy is most pronounced in finer-grained lithologies and less well developed in coarser-grained lithologies. Therefore, lithology and pervasive, sedimentological structure have a profound effect on the directional anisotropy of the electrical properties of geological materials.

Differences between measured electrical resistivity trends for each array are generally low, however, differences can be attributed to the volume of sample imaged by each array (smaller array will ‘sample’ a smaller volume of material). Smaller array sizes will be more greatly influenced by structures such as cracks and bedding planes. Larger arrays, on the other hand, will be more capable of averaging out sample structures.

In several instances, elevated 50 mm array resistivity measurements were associated with desiccation taking place along bedding planes within the samples. An example of where this process occurred is the siltstone of Sample 6 between 5% and 12% GMC.

Repeat measurement error is attributed to contact resistances and the electrode surface area available to make contact with the sample. Higher contact resistances are responsible for repeat measurement errors being highest at low moisture contents, whereas, measurement error is higher for the 10 mm array that the 50 mm array due to the former having a smaller surface area to make sample contact. Relatively low repeat measurement errors are exhibited at higher moisture contents because of the ease with which current is transmitted into and out of the samples.

### 4.2. Laboratory experimentation and modelling

Trough calibration using saline solution and subsequent application of a geometric factor and temperature correction enables a robust estimate of sample resistivity to be made. Field resistivity measurements also take into account both the geometry

of electrical measurements during the inversion process and temperature effects post-inversion by normalising field resistivity to a pre-defined temperature. Therefore the laboratory determined property relationships can be effectively applied to field resistivity results due to standardising the physical treatment of data.

Siltstone of Sample 6 experienced significant desiccation cracking during the drying phase of resistivity experimentation, which acted to increase resistivity at low GMC, and so rendered several measurements of resistivity-moisture content unrepresentative of the SSF as a whole. This could be resolved by performing electrical measurements on samples maintained at their in-situ confining pressures and applying an overburden load.

Where high %RMS misfit errors occur these are attributed to additional processes taking place in the samples which Waxman–Smits equation does not account for. For example, Sample 4, 10 mm array measurements have 4 measurements that fall below the expected resistivity curve and as a result a model fit error of 205%. The exact reason for this is unknown, but could be attributed to coarse sand-sized iron stone clasts permitting electronic conduction within the sample. However, this hypothesis may not be correct, as it is likely that electronic conductivity would affect measurements at all moisture contents.

Sample 3 is a free-draining, fine sand with a relatively low CEC (compared to other samples) and records high model misfit of between 68.2% and 132.8%. This apparently less well fitted model is potentially due to the sand developing a water table and therefore contains two zones with different GMCs. But could equally be explained by the existence of low clay content soils possessing a discontinuous electrical double layer (Wehrer et al., 2014).

### 4.3. Waxman–Smits equation and shrinkable clays

Samples that contained large proportions of clay minerals, Samples 1 and 2 in particular, experienced considerable shrinkage and swelling when drying and wetting the samples in the laboratory. The shrink-swell process has the effect of altering the porosity of the lithology, which has a profound effect on the sample porosity and therefore, the Waxman–Smits model. The degree of shrinkage and swelling of samples was measured throughout the laboratory experimentand porosity change (Fig.8a) was modelled (Head, 2002). The Waxman–Smits models were remodelled and taking into account the porosity variability and results are presented in Fig. 8. Accounting for shrinkage in clay-dominated lithologies creates models with lower %RMS errors, when compared to porosity constant Waxman–Smits models. Samples 1 and 2 both show a

reduction of 7.1% and 0.5% in %RMS error when porosity is incorporated into the electropetrophysical model.

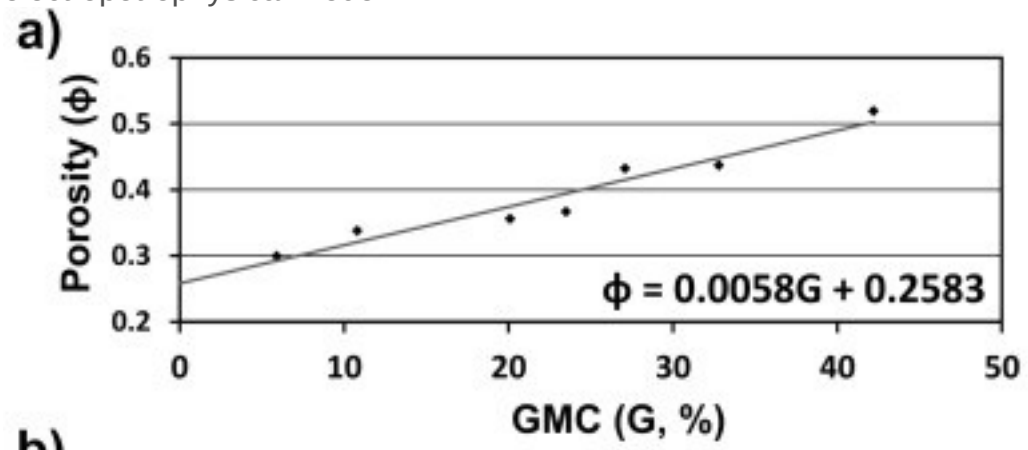


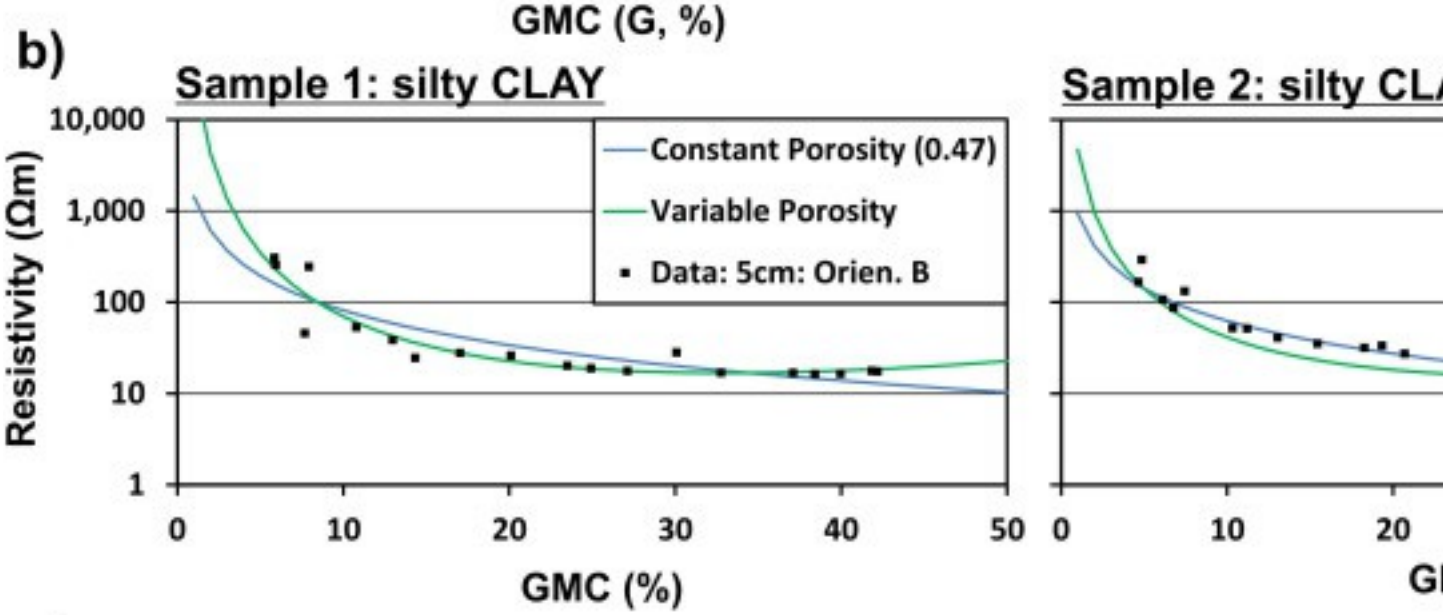


c)

| | Sample 1 | | Sample 2 | |
|---|---|---|---|---|
| | Constant $\phi$ | Variable $\phi$ | Constant $\phi$ | Variable $\phi$ |
| n | 2.2 | 4.1 | 2.2 | 3.4 |
| F | 30.0 | 42.8 | 25.1 | 36.5 |
| %rms | 50.6 | 43.5 | 18.5 | 18.0 |

1. Download high-res image (469KB)
2. Download full-size image

Fig. 8. Comparison between Waxman–Smits models between porosity-constant and porosity-variable models.

The porosity variable Waxman–Smits Model produces models that possess a resistivity increase at the highest soil moisture contents (< 35% GMC). This feature is not present

in measured electrical data and is therefore an artefact of the model. Despite the porosity variable petrophysical model producing models with slightly lower %RMS errors, it may be that assuming a porosity constant model is more indicative of real-world conditions.

### 4.4. Model parameter selection

Resistivity measurements utilising the 50 mm square array almost universally produce models with the lower %RMS errors than their 10 mm square array equivalent. In addition to selecting which resistivity measurement square array size to model when modelling resistivity—GMC relationships, the decision as to which resistivity measurement orientation to use, one of either orientations A, B or an arithmetic average of A and B had to be made.
The field resistivity measurements associated with this investigation are taken along 5 parallel lines which are installed – to within a few degrees – parallel to the maximum dip of the slope (12°). Earthflows are deposited roughly parallel to the slope surface, therefore, when field resistivity surveys are performed injected current is assumed to flow along bedding surfaces and flow slip surfaces. This hypothesis would justify the implementation of resistivity measurements utilising orientation A.

However, another argument exists for opting to use the mean averages of resistivities measured by orientations A and B. Field measurements of electrical resistance are modelled and in doing so converted to electrical resistivity through the inversion process. The inversion process takes a series of surface four-point measurements and builds a model of the subsurface structure which best-matches the raw surface field measurements. Conventional inversion algorithms do not account for anisotropy. It would therefore not increase the accuracy of ERT derived gravimetric moisture content results by generating orientationally specific data to an inverse model that does not accommodate the geometric subtleties of such data.

### 4.5. Soil moisture retention and resistivity

Soil matric suctions occur over a small moisture content range but over a large resistivity change in sandy material relative to clay rich material. Conversely, suction variation within clay occurs over a high range of moisture contents but a low range of resistivity. In terms of slope instability processes, suctions dissipate due to a smaller increase of GMC in the sand flow compared to the clay flow whose moisture contents dissipate over double the GMC range. Therefore, in order to monitor soil matric suction

evolution in a clay slope using ERT monitoring the system would have to be sufficiently sensitive so as to observe a small range of resistivity, as this equates to a wide range of matric suctions.

It should be noted that water-pressure-saturation relationships recreated in laboratory conditions are not fully representative of exact field conditions. This is because during pressure plate testing and sample re-wetting the natural pore structure of soils is destroyed.

## 5. Conclusions

Laboratory resistivity measurements show that the techniques utilised (samples and square array) have considerable potential as a means of electropetrophysical calibration of engineering soils and weak rock. However, suitability of results in light of issues such as sample cracking and electrical conduction must be identified and accounted for if the results are to be accurately up-scaled to inverted model resistivity results. The existence of directional anisotropy makes model calibration curve selection more difficult due to variability in the range of measured laboratory resistances.

However, use of the larger measurement array size means that experimental data will be more representative of bulk lithological properties. In addition, use of electrodes with a relatively high surface area (wide diameter) help maintain low contact resistances and repeat measurement error, relative to narrow electrodes.

Model fit varies widely, fit is best for clay-dominated WMF-derived samples but fits less well for sand-dominated samples. Waxman–Smits equation is appropriately applied in this investigation as all samples have considerable clay mineral content, as can is shown in non-negligible CEC results.

Incorporation of pressure plate, suction measurements on samples allows suction dissipation to be quantified and evaluated alongside moisture content.

## References


Archie, 1942

G.E. Archie**The electrical resistivity log as an aid in determining some reservoir characteristics**

Pet. Trans. AIME., 146 (1942), pp. 54-62

CrossRefView Record in Scopus

Barnes, 2010

G. Barnes**Soil Mechanics : Principles and Practice**
(third ed.), Palgrave Macmillan (2010)

Bell, 2007

F.G. Bell**Engineering Geology**
(second ed.), Elsevier, Butterworth-Heinemann (2007)

Binley et al., 2002

A. Binley, P. Winship, L.J. West, M. Pokar, R. Middleton**Seasonal variation of moisture content in unsaturated sandstone inferred from borehole radar and resistivity profiles**
J. Hydrol., 267 (3–4) (2002), pp. 160-172, 10.1016/S0022-1694(02)00147-6
(15 October, ISSN 0022-1694)
ArticleDownload PDFView Record in Scopus

Brovelli et al., 2005

A. Brovelli, G. Cassiani, E. Dalla, F. Bergamini, D. Pitea**Electrical properties of partially saturated sandstones: novel computational approach with hydrogeophysical applications**
Water Resour. Res., 41 (2005), p. W08411, 10.1029/2004WR003628

Brunet et al., 2010

P. Brunet, R. Clément, C. Bouvier**Monitoring soil water content and deficit using electrical resistivity tomography (ERT)—a case study in the Cevennes area, France**
J. Hydrol., 380 (1) (2010), pp. 146-153
ArticleDownload PDFView Record in Scopus

Cassiani et al., 2009

G. Cassiani, A. Godio, S. Stocco, A. Villa, R. Deiana, P. Frattini, M. Rossi**Monitoring the hydrologic behaviour of a mountain slope via time-lapse electrical resistivity tomography**
Near Surf. Geophys., 7 (5–6) (2009), pp. 475-486
View Record in Scopus

Chambers et al., 2014

J.E. Chambers, D.A. Gunn, P.B. Wilkinson, P.I. Meldrum, E. Haslam, S.Holyoake, M. Kirkham, O. Kuras, A. Merritt, J. Wragg**4D electrical resistivity tomography monitoring of soil moisture dynamics in an operational railway embankment**
Near Surf. Geophys., 12 (1) (2014), pp. 61-72, 10.3997/1873-0604.2013002
View Record in Scopus

Chambers et al., 2011

J.E. Chambers, P.B. Wilkinson, O. Kuras, J.R. Ford, D.A. Gunn, P.I.Meldrum, R.D. Ogilvy**Three-dimensional geophysical anatomy of an active landslide in Lias Group mudrocks, Cleveland Basin, UK**
Geomorphology, 125 (4) (2011), pp. 472-484
ArticleDownload PDFView Record in Scopus

Cruden and Varnes, 1996

D.M. Cruden, D.J. Varnes**Landslide types and processes**

Special Report 247: Landslides: Investigation and Mitigation, Washington D.C., Transportation Research Board (1996)

Di Maio and Piegari, 2011

R. Di Maio, E. Piegari**Water storage mapping of pyroclastic covers through electrical resistivity measurements**

J. Appl. Geophys., 75 (2) (2011), pp. 196-202

ArticleDownload PDFView Record in Scopus

Dijkstra and Dixon, 2010

T.A. Dijkstra, N. Dixon**Climate change and slope stability in the UK: challenges and approaches**

Q. J. Eng. Geol. Hydrogeol., 43 (4) (2010), pp. 371-385

CrossRefView Record in Scopus

Dijkstra et al., 2014

T.A. Dijkstra, J. Wasowski, M.G. Winter, X.M. Meng**Introduction to geohazards of Central China**

Q. J. Eng. Geol. Hydrogeol., 47 (3) (2014), pp. 195-199

CrossRefView Record in Scopus

Eichenberger et al

.
,
2
0
1
3

J. Eichenberger, A. Ferrari, L. Laloui**Early warning thresholds for partially saturated slopes in volcanic ashes**
Comput. Geotech., 49 (2013), pp. 79-89
ArticleDownload PDFView Record in Scopus

Friedel et al., 2006

S. Friedel, A. Thielen, S.M. Springman**Investigation of a slope endangered by rainfall-induced landslides using 3D resistivity tomography and geotechnical testing**
J. Appl. Geophys., 60 (2) (2006), pp. 100-114
ArticleDownload PDFView Record in Scopus

Glover et al., 2000

P.W. Glover, M.J. Hole, J. Pous**A modified Archie's law for two conducting phases**
Earth Planet. Sci. Lett., 180 (3) (2000), pp. 369-383
ArticleDownload PDFView Record in Scopus

Hayley et al., 20

K. Hayley, L.R. Bentley, M. Gharibi, M. Nightingale**Low temperature dependence of electrical resistivity: implications for near surface geophysical monitoring**
Geophys. Res. Lett., 34 (18) (2007)

Hayley et al., 20

K. Hayley, L.R. Bentley, A. Pidlisecky**Compensating for temperature variations in time-lapse electrical resistivity difference imaging**
Geophysics, 75 (4) (2010), pp. WA51-WA59
CrossRef

Head, 2002

K.H. Head**Manual of Soil Laboratory Testing**
(third ed.), Whittle Publishing (2002)

Jongmans and G

D. Jongmans, S. Garambois**Geophysical investigation of landslides: a review**
Bull. Soc. Geol. Fr., 178 (2) (2007), pp. 101-112
CrossRefView Record in Scopus

Lebourg et al., 2

T. Lebourg, S. Binet, E. Tric, H. Jomard, S. El Bedoui**Geophysical survey to estimate the 3D sliding surface and the 4D evolution of the water pressure on part of a deep seated landslide**
Terra Nova, 17 (5) (2005), pp. 399-406
CrossRefView Record in Scopus

Loke, 1997

M.H. Loke**Electrical Imaging Surveys for Environmental and Engineering Studies. A Practical Guide to**
(1997)

Loke et al., 2013

M.H. Loke, J.E. Chambers, D.F. Rucker, O. Kuras, P.B. Wilkinson**Recent developments in the direct-current geoelectrical imaging method**
J. Appl. Geophys., 95 (2013), pp. 135-156, 10.1016/J.Jappgeo.2013.02.017
(August, ISSN 0926-9851)
ArticleDownload PDFView Record in Scopus

Lourenço et al., 2

S.D.N. Lourenço, D. Gallipoli, D.G. Toll, C.E. Augarde, F.D. Evans**A new procedure for the determination of soil-water retention curves by continuous drying using high-suction tensiometers**
Can. Geotech. J., 48 (2) (2011), pp. 327-335
CrossRefView Record in Scopus

Merritt et al., 201

A.J. Merritt, J.E. Chambers, W. Murphy, P.B. Wilkinson, L.J. West, D.A. Gunn, P.I. Meldrum, M. Kirkham, N. Dixon**3D ground model development for an active landslide in Lias mudrocks using geophysical, remote sensing and geotechnical methods**
Landslides, 1-14 (2013), p. 14, 10.1007/s10346-013-0409-1
View Record in Scopus

Ntarlagiannis et

D. Ntarlagiannis, N. Yee, L. Slater**On the low-frequency electrical polarization of bacterial cells in sands**
Geophys. Res. Lett., 32 (24) (2005)

Revil and Glover

A. Revil, P.W.J. Glover**Nature of surface electrical conductivity in natural sands, sandstones, and clays**
Geophys. Res. Lett., 25 (5) (1998), pp. 691-694
CrossRefView Record in Scopus

Revil et al., 1998

A. Revil, L.M. Cathles, S. Losh, J.A. Nunn**Electrical conductivity in shaly sands with geophysical applications**
J. Geophys. Res. Solid Earth, 103 (B10) (1998), pp. 23925-23936
(1978–2012)
CrossRefView Record in Scopus

Russell and Bark

E.J. Russell, R.D. Barker**Electrical properties of clay in relation to moisture loss**
Near Surf. Geophys., 8 (2) (2010), pp. 173-180
View Record in Scopus

Shevnin et al., 20

V. Shevnin, A. Mousatov, A. Ryjov, O. Delgado-Rodriquez**Estimation of clay content in soil based on resistivity modelling and laboratory measurements**
Geophys. Prospect., 55 (2) (2007), pp. 265-275
CrossRefView Record in Scopus

Slater and Lesm

L.D. Slater, D. Lesmes**IP interpretation in environmental investigations**
Geophysics, 67 (1) (2002), pp. 77-88
CrossRefView Record in Scopus

Sorbino and Nico

G. Sorbino, M.V. Nicotera**Unsaturated soil mechanics in rainfall-induced flow landslides**
Eng. Geol., 165 (2013), pp. 105-132
ArticleDownload PDFView Record in Scopus

Supper et al., 20

R. Supper, D. Ottowitz, B. Jochum, J.H. Kim, A. Römer, I. Baron, S. Pfeiler, M. Lovisolo, S. Gruber, F. Vecchiotti**Geoelectrical monitoring: an innovative method to supplement landslide surveillance and early warning**
Near Surf. Geophys., 12 (1) (2014), pp. 133-150
View Record in Scopus

Telfold et al., 199

W.M. Telfold, L.P. Geldert, R.E. Sheriff**Appl. Geophys**
Cambridge Univ, New York (1991)

Toll et al., 2011

D.G. Toll, S.D.N. Lourenço, J. Mendes, D. Gallipoli, F.D. Evans, C.E. Augarde, Y.J. Cui, A.M. Tang, J.C. Rojas Vidovic, L. Pagano, C. Mancuso, C. Zingariello, A.Tarantino**Soil suction monitoring for landslides and slopes**
Q. J. Eng. Geol. Hydrogeol., 44 (1) (2011), pp. 23-33
CrossRefView Record in Scopus

Ulrich and Slater

C. Ulrich, L. Slater**Induced polarization measurements on unsaturated, unconsolidated sands**
Geophysics, 69 (3) (2004), pp. 762-771, 10.1190/1.1759462
CrossRefView Record in Scopus

Vanhala and Soi

H. Vanhala, H. Soininen**Laboratory technique for measurement of spectral induced polarization response of soil sampies**
Geophys. Prospect., 43 (5) (1995), pp. 655-676
CrossRefView Record in Scopus

Waxman and Sm

M.H. Waxman, L.J.M. Smits**Electrical conductivities in oil bearing sands**
J. Soc. Pet. Eng., 8 (1968), pp. 107-122
CrossRefView Record in Scopus

Wehrer et al., 20

M. Wehrer, H. Lissner, E. Bloem, French, K.U. Totsche**Electrical resistivity tomography as monitoring tool for unsaturated zone transport: an example of preferential transport of deicing chemicals**
Environ. Sci. Pollut. Res., 21 (15) (2014), pp. 8964-8980
(August)
CrossRefView Record in Scopus